Neoclassical transport in displaced tokamak helical cores

J. M. García-Regaña[1,2], H. Smith[3], Y. Turkin[3], M. Sertoli[2], C. Angioni[2], A. Bustos[3], W. A. Cooper[5], J. Geiger[3], R. Kleiber[3], E. Strumberger[2] and ASDEX Upgrade Team.

[1] *EUROfusion PMU, Garching b. München, Boltzmannstr. 2 85748, Germany*
[2] *Max-Planck-Institut für Plasmaphysik, Boltzmannstr. 2 85748, Garching b. München, Germany*
[3] *Max-Planck-Institut für Plasmaphysik, Wendelsteinstr. 1 17491, Greifswald, Germany*
[4] *Departamento de Física, Universidad Carlos III, Leganés, 28911, Spain*
[5] *Centre de Recherches en Physique des Plasmas, EPFL, CH-1015 Lausanne, Switzerland*

Introduction

Recent experiments in ASDEX Upgrade (AUG) have shown expulsion of Tungsten out of the helical core produced by internal (1,1) kink modes [1]. Given that impurities dilute the plasma fuel and cool it down due to their high radiative power, the identification of mechanisms that suppress or mitigate impurity accumulation is of central importance for the success of thermonuclear fusion.

Although tokamaks are nominally axi-symmetric, they are often subject to 3D perturbations, e.g. due to TF coil ripple, RMP coils used for ELM mitigation or, as in the aforementioned AUG experiments, developement of bifurcated helical MHD states. The loss of the toroidal symmetry of the magnetic field is recognized as potential overlap with the physics features and tools familiar to stellarators and a good basis for addressing the question of to what extent such physics features can show up in tokamaks. Following a similar reasoning, the closeness of stellarators to certain symmetries which make them exhibit tokamak properties like for instance large rotation, is currently an active research field [2]. In the present work we initiate the evaluation of some of these features in the frame of neoclassical theory, including the search for transport scaling at low collisionalities, estimation of the ambipolar electric field and potential variations. This preliminary assessment relies on the central motivation and mid-term objective of studying the dynamics of impurities in the aforementioned 3D tokamak equilibria.

The 3D AUG equilibrium considered

3D equilibrium tokamak states can be generated with the Variational Moments Equilibrium Code VMEC [3], prescribing the plasma boundary, pressure and toroidal current profiles as well as an initial non-planar axis guess. If parameters are such that a weakly reversed shear q profile with a minimum near unity is obtained and the axis guess is sufficiently distorted the output results in a 3D solution with helical core similar to a saturated $m/n = 1/1$ ideal internal

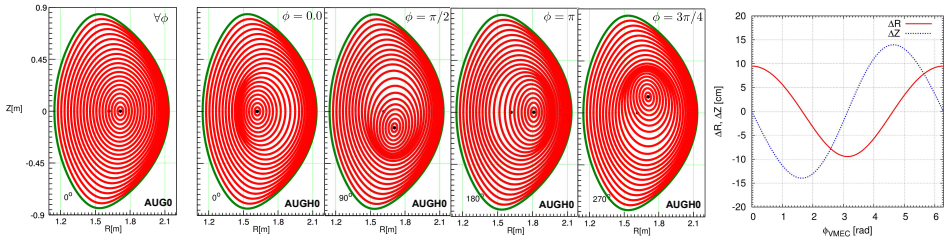

Figure 1: From left to right: Magnetic flux surface contours for the initial axi-symmetric AUG equilibrium (left-most figure); 3D final solution at 4 toroidal angles; and displacement of the axis along the cylindrical coordinates R and Z as a function of the toroidal VMEC coordinate.

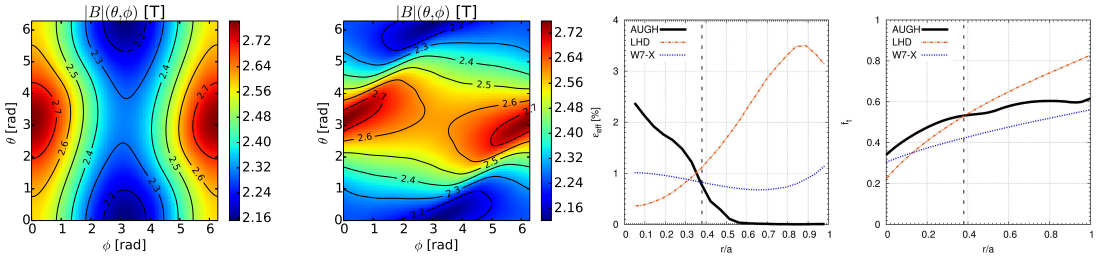

Figure 2: (Left to right) Modulus of B as a function of the PEST angular coordinates θ and ϕ at $r/a = 0.1$ and 0.35; ε_{eff} and f_t radial profiles for the 3D AUG equilibrium, $Wendeltstein7-X$ and LHD stellarator.

kink [4]. In the present study the plasma boundary corresponding to an perfectly axi-symmetric equilibrium of AUG has been considered (see left-most plot in fig. 1). The final developed 3D solution (see the 4 poloidal cross sections in fig. 1) shows a helical displaced core inside the $q = 1$ surface situated at the normalized effective radius $r/a \approx 0.4$. Finally the helical axis displacement amplitude (right-most plot of fig. 1) is approximately 10 and 12 cm along the usual cylindrical coordinates Z and R respectively.

Prior to quantitative neoclassical considerations, it is important to note that the equilibrium suffers a strong deviation from toroidal symmetry in the helical core, which is seen in the contour maps of the magnetic field strength in fig. 2. In addition, the fraction of trapped particles f_t and the effective ripple ε_{eff} take values of the order of or larger than stellarators like LHD and W7-X in their standard configurations.

Neoclassical simulations

Regarding the neoclassical simulations, these have been performed with the neoclassical version of the Monte-Carlo δf PIC code EUTERPE [5, 6]. In the most general case EUTERPE solves the drift kinetic equation including the potential varying on the flux surface Φ_1:

$$\frac{\partial f_1}{\partial t} + \dot{\mathbf{R}} \cdot \nabla f_1 + \dot{v}_{\parallel} \frac{\partial f_1}{\partial v_{\parallel}} = -f_{\text{M}} \left(\mathbf{v}_{\text{d}} + \mathbf{v}_{E1}\right) \cdot \nabla r \left[\frac{n'}{n} + \frac{q}{T}\Phi_0' + \left(\frac{mv^2}{2T} - \frac{3}{2} + \frac{q}{T}\Phi_1\right)\frac{T'}{T}\right],$$

with $' \equiv \mathrm{d}/\mathrm{d}r$, f_1 the departure from $f_0 = f_{\text{M}} \exp\left(-Z|e|\Phi_1/T\right)$, the lowest order distribution function; Φ_0 the ambipolar part of the electrostatic potential, v_{E1} the $E \times B$ drift related to Φ_1

and v_d the magnetic drift. The characteristics at lowest order are for the guiding center $\mathbf{R}$, parallel velocity $v_\parallel$ and magnetic moment μ: $\dot{\mathbf{R}} = v_\parallel \mathbf{b} - \frac{\nabla\Phi_0 \times \mathbf{B}}{B^2}$; $\dot{v}_\parallel = -\frac{Ze}{m}\mathbf{b}\cdot\nabla\Phi_1 - \mu\mathbf{b}\cdot\nabla B - \frac{v_\parallel}{B^2}(\mathbf{b}\times\nabla B)\cdot\nabla\Phi_0$; and $\dot{\mu} = 0$. Φ_1 is obtained after requiring quasi-neutrality up to first order among the involved species. The assumption of adiabatic electrons considered here leads to the equation: $\Phi_1 = \frac{T_e}{e}\left(n_{0e} + n_{0i}\frac{T_e}{T_i}\right)^{-1} n_{1i}$, with n_0 and n_1 the equilibrium and perturbed densities, T the temperature and $\{i, e\}$ the bulk ion and electron indices. The collisions (pitch angle scattering in the present work) are performed in each time-step applying a random kick in the markers' pitch angle after pushing them along the collisionless characteristics.

The collision frequency is defined as the sum over all the target species of the deflection collision frequency: $\nu = \sum_b \nu_D^{ab}$. To get a simplified picture of the physics, however, it can be set constant for all markers, which enables depicting the different collisional regimes participating in the transport processes. In particular for the above-mentioned AUG equilibrium and zero value of the radial electric field ($E_r = -\mathrm{d}\Phi_0/\mathrm{d}r$) the low collisional asymptotic $1/\nu$ regime shows up at the helical core for the transport matrix coefficient L_{11} [7] (see fig. 3 left), while the usual *banana* scaling is recovered at a more external radius (see fig. 3 right).

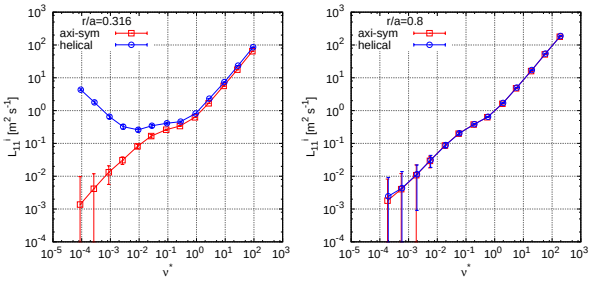

Figure 3: L_{11} transport matrix coefficient as a function of the normalized thermal collision frequency $\nu^* = \nu R_0 q/v_{\mathrm{th}}$ inside the helical core (left) and far outside (right).

Along the same line-of-thought, considering a set of analytical temperature and density profiles similar to those reported for the experimental AUG discharge #31114 in [1], see fig. 4(left), the neoclassical radial transport of bulk ions (H^+) for $E_r = 0$ is significantly larger – between two and three orders of magnitude – in the helical core region compared with the outer axisymmetric radii, regardless of the weaker gradients at the inner positions. This is observed in

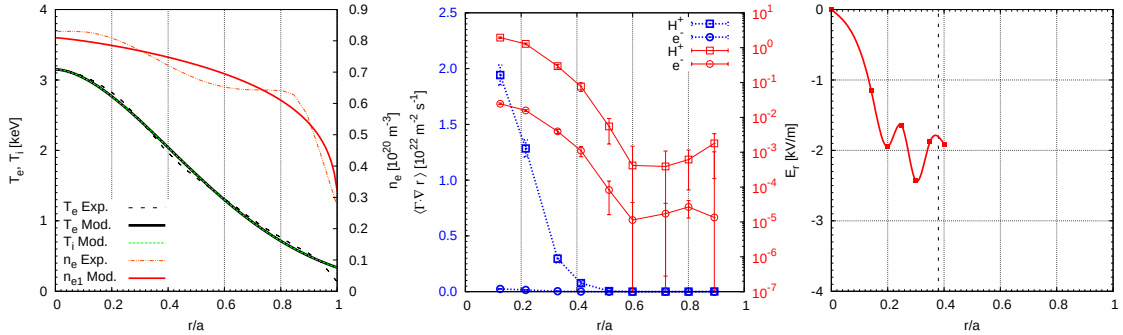

Figure 4: (Left) Plasma parameters fitted to AUG discharge #31114. (Center) Particle flux density of bulk ions (H^+) and electrons for $E_r = 0$ in logarithmic (red) and linear (blue) scales. (Right) Radial electric field estimation inside $q = 1$ surface.

fig. 4(center). Such large ion radial particle flux in comparison to that observed out of the helical core, which falls nearly to the noise level, can lead to the onset of an electric field in order to restore the subsequent strong lack of ambipolarity. The estimate of E_r is shown at different radii for a pure Hydrogen plasma in the displaced core in fig. 4(right).

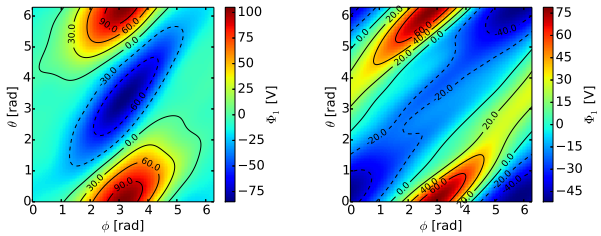

Figure 5: $\Phi_1(\theta,\phi)$ at $r/a = \{0.2, 0.35\}$.

Finally, in order to complete the picture for the electric field the potential variation within some flux surfaces at the displaced core has been obtained. This potential variation cannot be neglected, as is usually done, because the magnetic and electrostatic drifts become comparable as the charge state Z increases, which gives rise to an electrostatic transport source that can compete with the grad-B and curvature drives. A similar thing happens for the ratio between the magnetic and electrostatic mirror terms. As Z increases, electrostatic trapping becomes important, which affects the topology of the trapping boundaries set by the magnetic mirror term. In figure 5 the potential variation at $r/a = 0.2$ and 0.35 are represented. Considering the usual values obtained and measured [9, 10] in stellarators, these inside helical region are comparable and larger at similar collisionalities.

Conclusions

Considering this preliminary assessment of the magnitudes and properties relevant for 3D devices like ε_{eff}, presence of $1/\nu$ scaling, ambipolarity fulfillment and Φ_1 amplitude, the conclusion can be drawn that it would be questionable to apply an axi-symmetric approach to the helical state. Further studies involving the impact on impurity transport are ongoing.

Acknowledgements

This work has been carried out within the framework of the EUROfusion Consortium and has received funding from the Euratom research and training programme 2014-2018 under grant agreement No 633053. The views and opinions expressed herein do not necessarily reflect those of the European Commission.

References

[1] M. Sertoli *et al.*, this conference O4.129 (2015).
[2] I. Calvo *et al.* Plasma Phys. Control. Fusion **55** 125014 (2013).
[3] S. P. Hirshman *et al.* J. Comput. Phys. **96**, 99 (1991).
[4] W.A. Cooper *et al.* Nucl. Fusion **53**, 073021 (2013).
[5] V. Kornilov *et al.* Nucl. Fusion **45**, 238 (2005).
[6] J. M. García-Regaña *et al.* Plasma Phys. Control. Fusion **55** 074008 (2013).
[7] C. D. Beidler *et al.* Nucl. Fusion **51**, 076001 (2011).
[8] M. Sertoli *et al.* Nucl. Fusion **53**, 053015 (2013).
[9] J. M. García-Regaña *et al.* to be submitted to Plasma Phys. Control. Fusion, preprint: http://arxiv.org/abs/1501.03967.
[10] M.A. Pedrosa *et al.* Nucl. Fusion **55** 052001 (2015).